JACS
JOURNAL OF THE AMERICAN CHEMICAL SOCIETY
Communication
pubs.acs.org/JACS

Nucleic Acid–Metal Organic Framework (MOF) Nanoparticle Conjugates

William Morris,[†] William E. Briley,[§] Evelyn Auyeung,[‡] Maria D. Cabezas,[†] and Chad A. Mirkin*[,†]

[†]Department of Chemistry and International Institute for Nanotechnology, Northwestern University, 2145 Sheridan Road, Evanston, Illinois 60208, United States

[‡]Department of Materials Science and Engineering, Northwestern University, 2220 Campus Drive, Evanston, Illinois 60208, United States

[§]Interdepartmental Biological Sciences, Northwestern University, 2205 Tech Drive, Evanston, Illinois 60208, United States

Supporting Information

ABSTRACT: Nanoparticles of a metal–organic framework (MOF), UiO-66-N_3 ($Zr_6O_4OH_4(C_8H_3O_4–N_3)_6$), were synthesized. The surface of the MOF was covalently functionalized with oligonucleotides, utilizing a strain promoted click reaction between DNA appended with dibenzylcyclooctyne and azide-functionalized UiO-66-N_3 to create the first MOF nanoparticle–nucleic acid conjugates. The structure of the framework was preserved throughout the chemical transformation, and the surface coverage of DNA was quantified. Due to the small pore sizes, the particles are only modified on their surfaces. When dispersed in aqueous NaCl, they exhibit increased stability and enhanced cellular uptake when compared with unfunctionalized MOF particles of comparable size.

Three-dimensional nucleic acid based structures exhibit properties that are often very different from their linear forms.[1] For example, spherical nucleic acid (SNA)–gold nanoparticle conjugates, which are synthesized from citrate-stabilized gold nanoparticles and alkylthiol functionalized oligonucleotides (e.g. DNA or RNA), exhibit the unique ability to effectively enter cells without the use of cationic or viral transfection agents.[1a,2] Class A scavenger receptors on the surfaces of cells recognize the three-dimensional architecture and its densely packed oligonucleotide shell to facilitate their uptake via caveolin-mediated endocytosis.[3] Consequently, SNAs are the basis for many intracellular diagnostic, drug delivery, and gene regulation strategies.[4] In addition to enhanced cellular uptake, the resistance SNAs have to nuclease degradation and their lack of significant cellular cytotoxicity and immunogenicity make them particularly attractive for such applications.[5] The composition of the core in this process is not particularly important, and there are now SNAs with cores composed of silica, iron oxide, and CdSe that also show very effective entry across many different cell lines.[6] Even hollow architectures have been synthesized and shown to exhibit similar properties.[7]

Infinite coordination polymers (ICPs) and metal–organic frameworks (MOFs) in particular are attractive compositions for the cores of SNAs.[8] In principle, the framework can be composed of molecules and metal ions that are important in both chemical sensing and therapeutics, and the pores within such structures can act as a host to carry other materials into cells.[9] Significant advances have been made in controlling the size and shape of such particles, yet little has been done to investigate the chemical interface between nucleic acids and MOFs.[10] Herein, we report the synthesis and characterization of a new zirconium based framework, UiO-66-N_3 ($Zr_6O_4OH_4(C_8H_3O_4$-$N_3)$) (Scheme 1A), a structural analogue of UiO-66, that can be rapidly functionalized with oligonucleotides via Cu-free strained-alkyne click chemistry, a reaction which has been utilized to interface MOFs in the bulk with a variety of organic functionalities (Scheme 1A–C).[11] The oligonucleotides create a steric and electrostatic barrier that stabilizes the particles in high dielectric media and render them functional with respect to cellular entry. These constructs are the first covalently functionalized MOF nanoparticle–oligonucleotide conjugates reported in the literature.

Three different samples of UiO-66-N_3, which differ in average particle size (540, 19, and 14 nm, respectively), were synthesized via solvothermal synthesis utilizing acetic acid to modulate crystallite size.[12] Powder X-ray diffraction (PXRD) of all three samples revealed that the UiO-66-N_3 has a cubic **fcu** topology, with a unit cell parameter of 20.84(1) Å (Figure 1A). All particle sizes were determined by TEM (using a minimum of 50 nanoparticles). The sample with the largest particles 540 ± 50 nm was formed in a 47% by vol acetic acid/*N*,*N*-dimethylformamide (DMF) mixture (Figure 1B). To reduce the size of the MOF nanoparticle, the volume of acetic acid in the solvothermal reaction was decreased. For example, when the reaction was run in a 9% by vol acetic acid/DMF mixture, 19 ± 4 nm particles were obtained, and with a 7% by vol acetic acid/DMF mixture, 14 ± 2 nm particles were formed (Figure 1C and D). The yields for the solvothermal reactions were determined by ICP-MS analysis of Zr content of digested MOF samples; they were $4.0(1) \times 10^{10}$, $1.0(1) \times 10^{15}$, and $1.8(2) \times 10^{15}$ particles/mL for 540, 19, and 14 nm particles, respectively.

To synthesize the nucleic acid–MOF nanoparticle conjugates, UiO-66-N_3 MOF nanoparticles, regardless of size, were reacted with dibenzylcyclooctyne (DBCO) functionalized DNA (Scheme 1A). In a typical experiment, an aqueous solution of 14 nm particles (0.15 nmol in 0.5 mL) was added to an

Received: March 31, 2014
Published: May 12, 2014

   dx.doi.org/10.1021/ja503215w | *J. Am. Chem. Soc.* 2014, 136, 7261–7264

Scheme 1. Synthesis and DNA Functionalization of UiO-66-N_3 Nanoparticles[a]

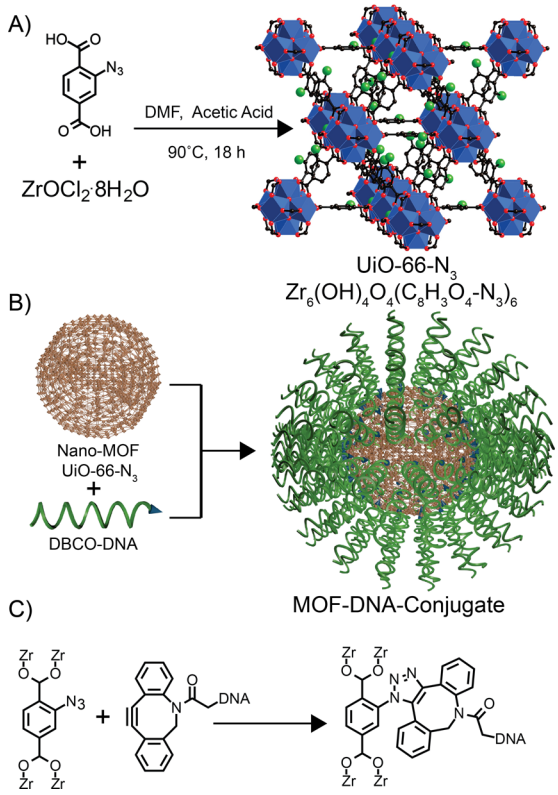

[a](A) Synthesis of UiO-66-N_3 ($Zr_6O_4OH_4(C_8H_3O_4\text{-}N_3)_6$) nanoparticles. (B) DNA functionalization of UiO-66-N_3 nanoparticles, utilizing DNA functionalized with dibenzylcyclooctyne (DBCO). (C) Strain promoted click reaction between a metal–organic framework (MOF) strut and DNA. Zirconium atoms = blue; oxygen atoms = red; carbon atoms = black; azide groups = green. Hydrogen atoms are omitted for clarity.

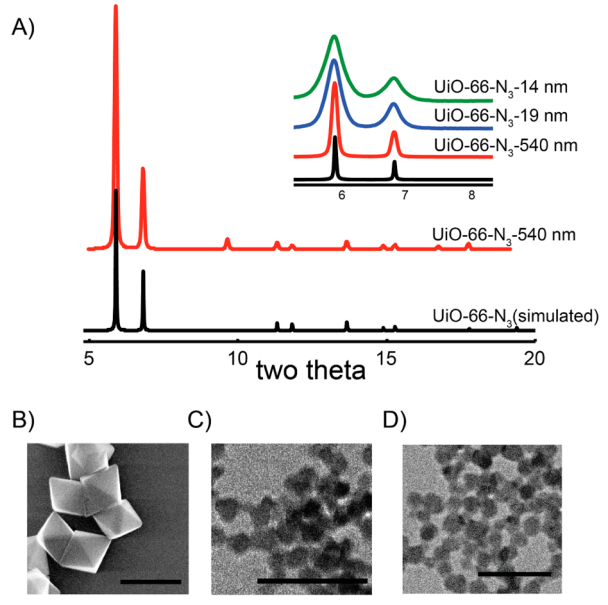

Figure 1. Characterization of UiO-66-N_3 nanoparticles: (A) Powder X-ray diffraction (PXRD) of simulated UiO-66-N_3 (black) and as synthesized UiO-66-N_3 540 nm MOF particles (red). (Inset) PXRD of MOF nanoparticles, simulated UiO-66-N_3 (black), UiO-66-N_3 540 nm MOF particles (red), as synthesized UiO-66-N_3, 19 nm MOF particles (blue), UiO-66-N_3 14 nm MOF particles (green). (B–D) SEM and TEM images of as synthesized MOF particles. Scale bar: 1 μm in B; 100 nm in C and D.

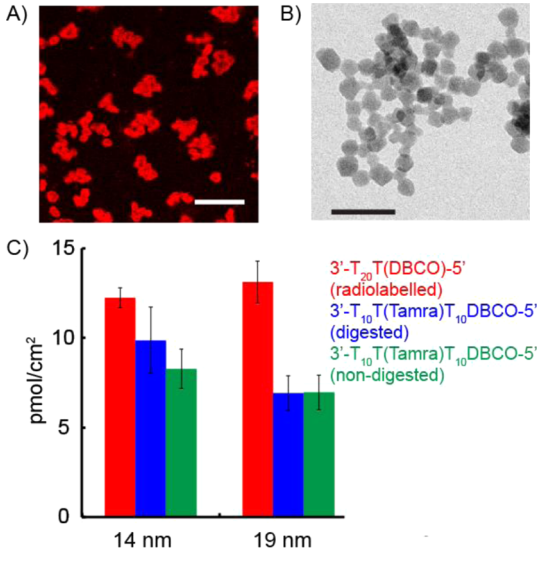

Figure 2. (A) Confocal microscopy of 540 nm MOF nanoparticle–DNA conjugates functionalized with TAMRA-labeled DNA. (B) Transmission electron microscopy of 19 nm MOF nanoparticle–DNA conjugates. Scale bar: 10 μm in A, 100 nm in B. (C) Nucleic acid surface densities of MOF nanoparticle–DNA conjugates.

aqueous solution of DNA (25 nmol in 1 mL) and mixed on a mechanical shaker for 72 h at 40 °C. Then, NaCl was slowly added to the solution to a final concentration of 0.5 M. The NaCl reduces electrostatic interactions between neighboring oligonucleotide strands allowing one to achieve higher surface densities of DNA. Free oligonucleotides were removed by centrifugation (3 × 15 000 rpm for 90 min), followed by resuspension of the MOF nanoparticle–oligonucleotide conjugates in H_2O.

Confocal microscopy of 540 nm particles functionalized with dye-labeled DNA shows that they are highly fluorescent, a consequence of DNA functionalization of the MOF surface (Figure 2A). TEM and PXRD after purification showed that the morphology and structure of the nanoparticles were maintained throughout the DNA functionalization process (Figure 2B).[12] Furthermore, measurements of the zeta potential showed a decrease from −27(5) to −41(6) and from −24(11) to −37(7) mV for 14 and 19 nm particles, respectively. Negative zeta potentials (<−30 mV) are indicative of nanoparticles functionalized with DNA.[1a,5,7]

In addition to the size of the nanoparticle–nucleic acid conjugates, the surface density is also important. Therefore, the surface coverage of DNA strands was investigated utilizing both radiolabeling and UV–vis absorbance techniques (Figure 2C). In the case of absorbance, a DNA strand consisting of two stretches of 10 bases separated by a dye, Tamra-dT, and terminated with DBCO was used to prepare the particles ($3'T_{10}T(Tamra)T_{10}$-DBCO$5'$). The dye concentration was determined both on the particle and after digestion of the particles in 0.1 M NaOH for 18 h, which degrades the MOF nanoparticle without significantly affecting the absorbance of the dye molecule at 556 nm.[12] Absorbance measurements of digested particles and intact structures were in good agreement

dx.doi.org/10.1021/ja503215w | J. Am. Chem. Soc. 2014, 136, 7261–7264

(Figure 2C). In addition, the DNA concentration was determined by ^{32}P radiolabeling of the 5′ terminus of a DNA strand (3′T_{20}T(DBCO)5′), which showed a higher loading of MOF nanoparticles when compared to the dye labeled DNA, 12.3(6) and 8.2(1.0) pmol/cm^2 per particle, respectively for 14 nm particles (Figure 2C). The difference in loading on MOF nanoparticles is attributed to the sterically bulky dye, which results in lower loading. For other nanoparticle−nucleic acid conjugates, changes in sequence design have been shown to greatly affect the loading of gold nanoparticles with DNA.[14] Loadings of 12.3(6) and 13.0 (1) pmol/cm^2 for MOF nanoparticle−DNA conjugates functionalized with (3′T_{20}T-(DBCO)5′) correspond to 5×10^{-10} ng of DNA/nanoparticle and 1×10^{-9} ng of DNA/nanoparticle for 14 and 19 nm MOF nanoparticle−DNA conjugates, respectively.

Previous studies have shown that the properties of SNAs are vastly different when compared to the unfunctionalized nanoparticle core. Two properties that change dramatically are the colloidal stability of SNAs and their ability to enter cells without transfection agents. Therefore, we compared the colloidal stability of MOF−DNA constructs with MOF nanoparticles by DLS at 37 °C (Figure 3A−E). DLS revealed that both MOF nanoparticles and MOF nanoparticle−DNA conjugates were colloidally stable in H_2O. However, upon addition of NaCl, MOF nanoparticles aggregate immediately, whereas MOF nanoparticle−DNA conjugates are stable up to 0.4 M NaCl before aggregation is observed (Figure 3A−E). This is due to the steric and electrostatic barriers to aggregation provided by the nucleic acid modified nanoparticle surface.

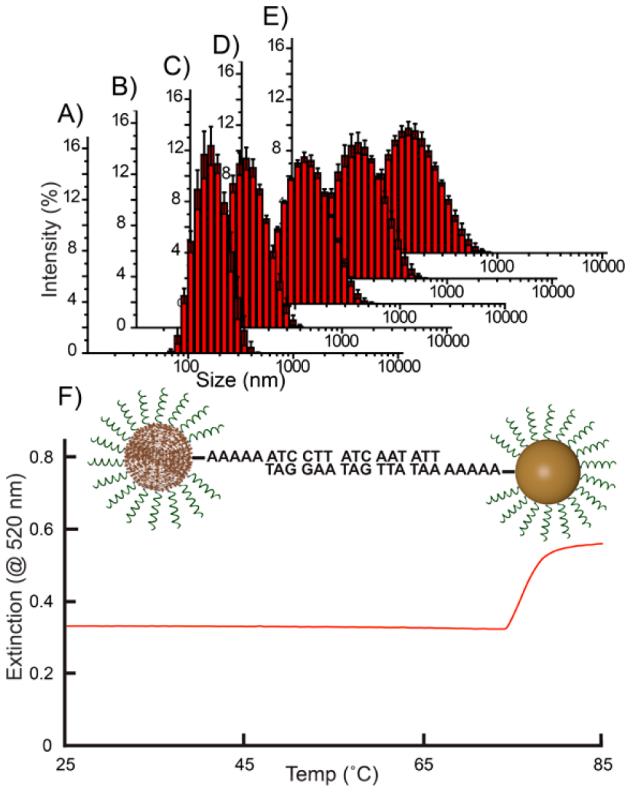

Figure 3. Dynamic light scattering data for (A) 14 nm MOF particles suspended in H_2O; (B) 14 nm MOF nanoparticle−DNA conjugates suspended in H_2O; (C) 14 nm MOF nanoparticle−DNA conjugates suspended in 0.1 M NaCl; (D) 14 nm MOF nanoparticle−DNA conjugates suspended in 0.2 M NaCl; and (E) 14 nm MOF nanoparticle−DNA conjugates suspended in 0.4 M NaCl. (F) Melting analysis at 520 nm for MOF nanoparticle−DNA conjugates and gold nanoparticle−DNA conjugates functionalized with complementary DNA.

A key consideration of these novel conjugates is their ability to hybridize in a sequence-specific fashion with complementary nucleic acids. To probe this issue, we allowed MOF nanoparticles functionalized with DNA to hybridize with 15 nm gold nanoparticles functionalized with complementary DNA. Subsequent melting analyses (monitoring at 520 nm) revealed a narrow melting transition (FWHM of the first derivative ≈ 3 °C), indicative of cooperative melting behavior, a hallmark characteristic of nucleic acid−nanoparticle conjugates (Figure 3F).[13] As expected, control experiments with non-complementary structures do not exhibit aggregation and subsequent melting.[12]

As previously stated, a key characteristic of SNAs is their ability to be naturally internalized by cells without the need for ancillary transfection agents.[1a,2−7] Therefore, the cellular uptake properties of these novel MOF nanoparticle−DNA conjugates was evaluated with HeLa (human cervical cancer) cells (Figure 4). HeLa cells were first incubated with MOF nanoparticle−DNA conjugates functionalized with Tamra-labeled DNA for 24 h and directly compared to free Tamra-labeled DNA at the same concentration (100 nM). Confocal microscopy revealed a high level of fluorescence in cells treated with MOF nanoparticle−DNA conjugates when directly compared to cells treated with free DNA (Figure 4A). To quantify this fluorescence, flow cytometry was carried out, which showed a 6-fold increase in fluorescence in cells treated with MOF nanoparticle−DNA conjugates when compared to free DNA. The cell uptake was also investigated by analyzing the zirconium content of cells treated with nanoparticles by ICP-MS. Cells were treated with a solution containing 1×10^{-7} mol/mL of zirconium, which corresponds to 25 and 12 pmol/mL for 14 and 19 nm particles, respectively. The cells treated with MOF nanoparticle−DNA conjugates showed higher zirconium concentrations than cells treated with the unfunctionalized nanoparticles, with 5×10^6 and 5×10^5 nanoparticles per cell for 14 and 19 nm MOF nanoparticle−

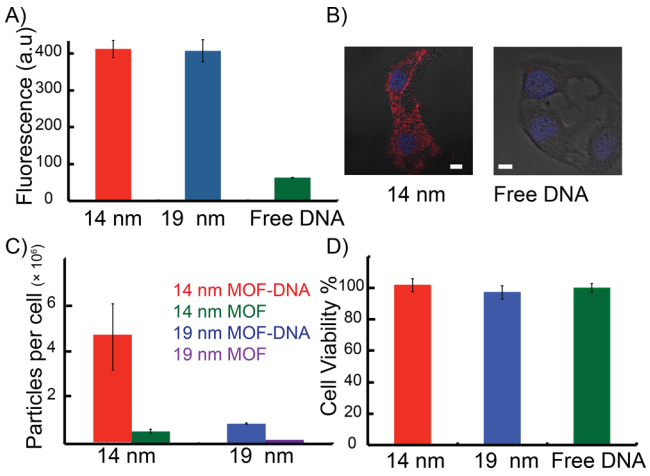

Figure 4. (a) Cell uptake by flow cytometry. (b) Confocal microscopy of cells treated with 14 nm MOF nanoparticle−DNA conjugates and with free DNA. Scale bar = 10 μm. (c) Nanoparticle uptake per cell determined by ICP-MS. (d) Cell viability assay data showing no significant cell toxicity for the MOF nanoparticle−DNA conjugates.

dx.doi.org/10.1021/ja503215w | J. Am. Chem. Soc. 2014, 136, 7261−7264

DNA conjugates, respectively (Figure 4C). Finally, the cell viability was assessed using a Presto Blue assay, which revealed that no significant cell death had occurred after 24 h of incubation (Figure 4D).

In conclusion, we have reported a novel class of nucleic acid−MOF nanoparticle conjugates, formed through a covalent coupling strategy, and have explored their colloidal stability and cellular transfection capabilities, which are dramatically different when compared to unfunctionalized MOF nanoparticles. This work is important because it creates a new and modular class of nanostructure that can be used in principle for many purposes, including as programmable atom equivalents in nucleic acid based assembly strategies and as intracellular delivery agents where both the nature of the oligonucleotide layer and MOF composition could be useful.[1a,15] When the principles and discoveries reported herein are extended to the many other types of MOFs and related porous materials, this class of nanostructure is likely to have a significant impact in various areas of chemistry, biology, and materials science.[8,16] Note that parallel efforts focused on the electrostatic attachment of siRNA to MOF nanoparticles recently appeared in the literature and has shown promise for intracellular gene regulation applications.[17]

■ ASSOCIATED CONTENT

Ⓢ Supporting Information

Full synthetic and analytic details. This material is available free of charge via the Internet at http://pubs.acs.org.

■ AUTHOR INFORMATION

Corresponding Author

chadnano@northwestern.edu

Notes

The authors declare no competing financial interest.

■ ACKNOWLEDGMENTS

This material is based upon work supported by the following awards: AFOSR under Award Nos. FA9550-11-1-0275 and FA9550-12-1-0280, and DARPA Award No. HR0011-13-2-0018. The content of the information does not necessarily reflect the position or the policy of the Government, and no official endorsement should be inferred. W.B. acknowledges a Northwestern University Ryan Fellowship. E.A. acknowledges a National Defense Science and Engineering Graduate (NDSEG) Fellowship (Number 32 CFR 168a).

■ REFERENCES

(1) (a) Cutler, J. I.; Auyeung, E.; Mirkin, C. A. *J. Am. Chem. Soc.* **2012**, *134*, 1376. (b) Breaker, R. R. *Nature* **2004**, *432*, 838. (c) Wang, Y.; Wang, Y.; Breed, D. R.; Manoharan, V. N.; Feng, L.; Hollingsworth, A. D.; Weck, M.; Pine, D. J. *Nature* **2012**, *491*, 51. (d) Seeman, N. C. *Annu. Rev. Biochem.* **2010**, *79*, 65.

(2) (a) Rosi, N. L.; Giljohann, D. A.; Thaxton, C. S.; Lytton-Jean, A. K. R.; Han, M. S.; Mirkin, C. A. *Science* **2006**, *312*, 1027. (b) Mirkin, C. A.; Letsinger, R. L.; Mucic, R. C.; Storhoff, J. J. *Nature* **1996**, *382*, 607.

(3) Choi, C. H. J.; Hao, L.; Narayan, S. P.; Auyeung, E.; Mirkin, C. A. *Proc. Natl. Acad. Sci. U.S.A.* **2013**, *10*, 7625.

(4) (a) Dhar, S.; Daniel, W. L.; Giljohann, D. A.; Mirkin, C. A.; Lippard, S. J. *J. Am. Chem. Soc.* **2009**, *131*, 14652. (b) Seferos, D. S.; Giljohann, D. A.; Hill, H. D.; Prigodich, A. E.; Mirkin, C. A. *J. Am. Chem. Soc.* **2007**, *129*, 15477. (c) Zhang, X.-Q.; Xu, X.; Lam, R.; Giljohann, D.; Ho, D.; Mirkin, C. A. *ACS Nano* **2011**, *5*, 6962. (d) Prigodich, A. E.; Randeria, P. S.; Briley, W. E.; Kim, N. J.; Daniel, W. L.; Giljohann, D. A.; Mirkin, C. A. *Anal. Chem.* **2012**, *84*, 2062.

(5) Seferos, D. S.; Prigodich, A. E.; Giljohann, D. A.; Patel, P. C.; Mirkin, C. A. *Nano Lett.* **2008**, *9*, 308.

(6) (a) Cutler, J. I.; Zheng, D.; Xu, X.; Giljohann, D. A.; Mirkin, C. A. *Nano Lett.* **2010**, *10*, 1477. (b) Young, K. L.; Scott, A. W.; Hao, L.; Mirkin, S. E.; Liu, G.; Mirkin, C. A. *Nano Lett.* **2012**, *12*, 3867.

(7) Cutler, J. I.; Zhang, K.; Zheng, D.; Auyeung, E.; Prigodich, A. E.; Mirkin, C. A. *J. Am. Chem. Soc.* **2011**, *133*, 9254.

(8) (a) Oh, M.; Mirkin, C. A. *Nature* **2005**, *438*, 651. (b) Spokoyny, A. M.; Kim, D.; Sumrein, A.; Mirkin, C. A. *Chem. Soc. Rev.* **2009**, *38*, 1218. (c) Furukawa, H.; Cordova, K. E.; O'Keeffe, M.; Yaghi, O. M. *Science* **2013**, 341. (d) Li, H.; Eddaoudi, M.; O'Keeffe, M.; Yaghi, O. M. *Nature* **1999**, *402*, 276.

(9) (a) Horcajada, P.; Gref, R.; Baati, T.; Allan, P. K.; Maurin, G.; Couvreur, P.; Férey, G.; Morris, R. E.; Serre, C. *Chem. Rev.* **2011**, 112−1232. (b) Foucault-Collet, A.; Gogick, K. A.; White, K. A.; Villette, S.; Pallier, A.; Collet, G.; Kieda, C.; Li, T.; Geib, S. J.; Rosi, N. L.; Petoud, S. *Proc. Natl. Acad. Sci. U.S.A.* **2013**, *110*, 17199. (c) Rieter, W. J.; Taylor, K. M. L.; Lin, W. *J. Am. Chem. Soc.* **2007**, *129*, 9852. (d) Taylor-Pashow, K. M. L.; Rocca, J. D.; Xie, Z.; Tran, S.; Lin, W. *J. Am. Chem. Soc.* **2009**, *131*, 14261.

(10) (a) Hermes, S.; Witte, T.; Hikov, T.; Zacher, D.; Bahnmüller, S.; Langstein, G.; Huber, K.; Fischer, R. A. *J. Am. Chem. Soc.* **2007**, *129*, 5324. (b) Schaate, A.; Roy, P.; Godt, A.; Lippke, J.; Waltz, F.; Wiebcke, M.; Behrens, P. *Chem.—Eur. J.* **2011**, *17*, 6643. (c) Sindoro, M.; Yanai, N.; Jee, A.-Y.; Granick, S. *Acc. Chem. Res.* **2014**, *47*, 459. (d) Guo, J. F.; Li, C. M.; Hu, X. L.; Huang, C. Z.; Li, Y. F. *RSC Adv.* **2014**, *4*, 9379. (e) Zhu, X.; Zheng, H.; Wei, X.; Lin, Z.; Guo, L.; Qiu, B.; Chen, G. *Chem. Commun.* **2013**, *49*, 1276.

(11) (a) Cavka, J. H.; Jakobsen, S.; Olsbye, U.; Guillou, N.; Lamberti, C.; Bordiga, S.; Lillerud, K. P. *J. Am. Chem. Soc.* **2008**, *130*, 13850. (b) Liu, C.; Li, T.; Rosi, N. L. *J. Am. Chem. Soc.* **2012**, *134*, 18886. (c) Wang, Z.; Liu, J.; Arslan, H. K.; Grosjean, S.; Hagendorn, T.; Gliemann, H.; Bräse, S.; Wöll, C. *Langmuir* **2013**, *29*, 15958.

(12) See Supporting Information for information on synthesis, DNA functionalization, and characterization of MOFs.

(13) Elghanian, R.; Storhoff, J. J.; Mucic, R. C.; Letsinger, R. L.; Mirkin, C. A. *Science* **1997**, *277*, 1078.

(14) Hurst, S. J.; Lytton-Jean, A. K. R.; Mirkin, C. A. *Anal. Chem.* **2006**, *78*, 8313.

(15) (a) Macfarlane, R. J.; O'Brien, M. N.; Petrosko, S. H.; Mirkin, C. A. *Angew. Chem., Int. Ed.* **2013**, *52*, 5688. (b) Macfarlane, R. J.; Lee, B.; Jones, M. R.; Harris, N.; Schatz, G. C.; Mirkin, C. A. *Science* **2011**, *334*, 204.

(16) (a) Kitagawa, S.; Kitaura, R.; Noro, S.-i. *Angew. Chem., Int. Ed.* **2004**, *43*, 2334. (b) Uemura, T.; Kitagawa, S. *Chem. Lett.* **2005**, *34*, 132. (c) Côté, A. P.; El-Kaderi, H. M.; Furukawa, H.; Hunt, J. R.; Yaghi, O. M. *J. Am. Chem. Soc.* **2007**, *129*, 12914.

(17) He, C.; Lu, K.; Liu, D.; Lin, W. *J. Am. Chem. Soc.* **2014**, *136*, 5181.

■ NOTE ADDED AFTER ASAP PUBLICATION

Scheme 1 contained errors in the version published ASAP May 12, 2014; the correct version reposted May 13, 2014.